International Journal of Lightweight Materials and Manufacture 3 (2020) 198–203

Contents lists available at ScienceDirect

International Journal of Lightweight Materials and Manufacture

journal homepage: https://www.sciencedirect.com/journal/international-journal-of-lightweight-materials-and-manufacture

Original Article

The composition design and properties investigation of Al-based amorphous powder

Lei Jin [a, b, *], Zhigang Che [a], Le Zhang [a], Bo Zhang [b], Zishuan Fan [c], Yanwen Chen [c]

[a] Science and Technology on Power Beam Process Laboratory, AVIC Manufacturing Technology Institute, Beijing, 100024, China
[b] Department of Materials Application Research, AVIC Manufacturing Technology Institute, Beijing, 100024, China
[c] School of Material Science and Technology, University of Science and Technology, Beijing, 100083, China

ARTICLE INFO

Article history:
Received 22 September 2019
Received in revised form
1 December 2019
Accepted 2 December 2019
Available online 12 December 2019

Keywords:
Al-based amorphous strip
Additive elements
Glass forming ability
Powder
Properties
Cold spray

ABSTRACT

By adding different amounts of rare earth element Y and Gd in $Al_{86}Ni_8Co_1La_5$, aluminum amorphous ribbon samples were prepared using single roller melt-spinning under 2 different roller speeds. Then X-ray diffraction (XRD), transmission electron microscope (TEM) and differential scanning calorimetry (DSC) were adopted to study the effect of rare earth element Y and Gd additions on phase structure, forming ability and thermal stability of $Al_{86}Ni_8Co_1La_5$ alloy. The results show that the better chemical composite is $Al_{86}Ni_8Co_1La_1Y_2Gd_2$, which can form a whole amorphous strip when the roller speed is 3 m/s. After the better chemical composition is confirmed, the Al-based amorphous powder is produced using gas atomization and its properties are also validated using cold spray technique. The thickness, porosity and amorphous amount of coatings is about 600 μm, 0.5% and 80.2% (CS–C), respectively. These findings indicate that $Al_{86}Ni_8Co_1La_1Y_2Gd_2$ amorphous powder can be used as raw materials for cold spray technique.

1. Introduction

Al-based bulk metallic glasses (BMGs) have exhibited high strength (above 1000 MPa, 3–4 times higher than crystalline counter parts), low density (3.2–3.7 g/cm^3), and better corrosion and wear properties [1–4]. Unfortunately, Al-based BMGs (or amorphous) are difficult to manufacture due to poor glass forming ability (GFA). So far, many efforts have been made to synthesize better Al-based BMGs with improved GFA [5–9]. How the advantages are kept and the disadvantages are avoided further for Al-based BMGs in industry? Among many methods, cold spray (CS) has proved to be an effective technique. It can deposit coatings through solid-state plastic deformation of micrometer scaled particles generating high strain rate (10^7-10^9 s^{-1}) at impact, which keeps the amorphous structure very well [10–12]. Combing amorphous powder and CS technology becomes a wonderful approach to fabricate Al-based amorphous material (coatings, like BMGs). For example, D. Lahiri et al. [13] prepared amorphous powder and sprayed them on 6061 aluminum. Their results indicate that the ability of corrosion and friction of amorphous coatings improve by 5 and 6 times, respectively. H.W. Zhang et al. [14] also found that $Al_{85}Ni_5Y_{10}$ amorphous alloy had better anticorrosion properties than those of pure Al and 2024 aluminum alloys in 0.25 mol/L NaOH and 1 mol/L HCl liquor.

Most of the present reports refer to less Al-based amorphous strip, powder and the corresponding coatings. Some scientists don't describe, composition design and the detail chemical composition of Al-based amorphous powder for CS process. What's the best chemical composition will be chosen for Al-based amorphous in CS process? It is very necessary and important to prepare Al-based amorphous powder which should have some characteristic with toughness, plastic and better amorphous stability.

According to previous references [15], $Al_{86}Ni_8Co_1La_5$ basic material is adopted and it will be ameliorated further in this investigation. Previous scientists, X.H. Fan et al. [16] found that Y can improve super-cooling liquid zone ΔT (about 72.42 K) and the amorphous formation ability when 3%Y is adopted. Y. Wang et al. [17] also found that Y has bigger atom radius and it possess higher negative mix enthalpy with Al and Ni atom. Therefore, Y can

* Corresponding author. Science and Technology on Power Beam Process Laboratory, AVIC Manufacturing Technology Institute, Beijing, 100024, China.
E-mail address: yugongyishanjin@126.com (L. Jin).

Peer review under responsibility of Editorial Board of International Journal of Lightweight Materials and Manufacture.

https://doi.org/10.1016/j.ijlmm.2019.12.001

substitute rare earth element La to strengthen amorphous formation ability. Besides, T. Mika et al.'s [15] investigations found that Gd not only improves the formation ability, but also enhances stability and increases crystal temperature of Al based amorphous. Z. Ling et al. [18] and other investigators also obtained the same phenomena and conclusions. That is, Gd is also a good additive and can improve the amorphous form ability. However, the effects of Y and Gd amount on $Al_{86}Ni_8Co_1La_5$ have never been involved so far. Therefore, the aim of this study is to investigate the effects of the important element Y and Gd on $Al_{86}Ni_8Co_1La_5$. Key properties, such as amount of amorphous strip, size, and high temperature phase stability and so on, are discussed systemically. The final aim of our laboratory is to produce Al-based amorphous powder which can be applied in CS process and prepared easily in future industrial production.

2. Experimental

2.1. Composites design of amorphous strip

Both Y and Gd were added into $Al_{86}Ni_8Co_1La_5$. Firstly, $Al_{86}Ni_8Co_1La_{5-x}Y_x$ was studied, and Y was added by 0 at.%, 2 at.%, 4 at.%, respectively. The purities of all of the raw materials were larger than 99.9%. The master alloys were remelted four times for composition homogeneity under argon atmosphere. Then thin amorphous alloy film samples (ribbon) were prepared using the single roller melt spinning method. The quenching rate was approximately expressed by the linear velocity of the copper roller. Quenching rates used in the experiment were 5 and 3 m s^{-1}, respectively.

2.2. Amorphous powder synthesis

After the chemical compositions of amorphous strip were affirmed, the same compositions alloys were atomized under Ar gas by the gas pulverization way. The technical parameters (four aspects) were listed as follows: (1) the ingredients were mixed according to the compositions design of amorphous strip and then all of the ingredients were placed in the induction crucible (about 1500 °C); (2) vacuum is pumped and crucible was filled with argon for protection and alloy materials were melted under 10^{-2} Pa; (3) argon atomization: alloy solution is atomized into small droplets under high pressure argon flow (2.0 MPa) and finally they were cooled to form amorphous powder; (4) powder screening: collecting −500 mesh for testing, analysis and spray.

2.3. Coatings prepared

The aimed amorphous coatings were prepared using the DWCS-2000 Cold Spraying System (Shanxi DW Automation Co., Ltd, China) with a maximum operating pressure of 4 MPa, temperature of 800 °C and operated with nitrogen as the propellant gas. Spraying distance (30 mm), spray gun velocity (300 mm/s) and powder velocity (20 g/s), powder size (10–25 μm) were fixed and just the spraying temperatures were adjusted (400 °C, 500 °C, 600 °C), which were marked as CS-A, CS-B, CS-C, respectively.

2.4. Properties measurements

The phase evolution was characterized by X-ray diffraction (XRD) using Philips diffractometer CuKα radiation. The microstructure of the ribbons was examined by transmission electron microscopy (TEM, JEM-ARM200F). The thermal behavior of the ribbons and powder was investigated by thermogravimetric-differential scanning calorimetry (TG-DSC, Pyris-7 produced by PerkinElmer) with different heating rate (10, 15, 20 and 30 K/min) in a flowing argon atmosphere. The morphology of the powder and coatings was characterized by scanning electron microscopy (SEM, ZEISS super-55 and LEO-1450) and the porosity of coatings was measured using Image J image analysis software. Usually, the image area was collected, then gray level difference analysis method was adopted, lengths, angles and porosity were measured, calculated and calibrate.

3. Results and discussion

3.1. Effect of Y amount on the amorphous forming ability

$Al_{86}Ni_8Co_1La_5$ alloy ribbons were prepared under 5 m/s and 3 m/s, and their XRD patterns were shown in Fig. 1. It showed that the position of $2\theta = 38°$ appeard the typical amorphous dispersion peaks, although some locations also appeard the crystal peaks. However, $Al_{86}Ni_8Co_1La_5$ alloy could form abundant amorphous structures and the prepared ribbons were also very thick (234 μm for 5 m/s, 123 μm for 3 m/s). Therefore, $Al_{86}Ni_8Co_1La_5$ was a good candidate material for amorphous structure.

In order to improve the amorphous ability of $Al_{86}Ni_8Co_1La_5$ alloy, Y was adulterated and the XRD patterns of $Al_{86}Ni_8Co_1La_{5-x}Y_x$ ($x = 0, 2, 4$) under 5 m/s and 3 m/s were shown in Fig. 2. It could be seen that $Al_{86}Ni_8Co_1La_{5-x}Y_x$ ($x = 0$) contained the mix phase of α-Al, Al_4CoLa and Al_4La phase. However, $Al_{86}Ni_8Co_1La_{5-x}Y_x$ ($x = 2, 4$) came out the obvious amorphous diffract peaks, which indicated that the additive Y assuredly help to produce amorphous phases. In order to further investigate which composition for $Al_{86}Ni_8Co_1La_{5-x}Y_x$ ($x = 2, 4$) has the best amorphous form ability, the 3 m/s were adopted and compared. Simultaneity, its XRD patterns were shown in Fig. 2b, which cleanly showed that $Al_{86}Ni_8Co_1La_1Y_4$ ($x = 4$) is better than that of $Al_{86}Ni_8Co_1La_{5-x}Y_x$ ($x = 0, 2$). These results indicated that Y could improve the amorphous formation ability of $Al_{86}Ni_8Co_1La_5$ although the lower rotation velocity was adopted (3 m/s).

3.2. Effect of Gd amount on the amorphous forming ability

5 different Gd contents were doped in $Al_{86}Ni_8Co_1La_1Y_4$. That is, $Al_{86}Ni_8Co_1La_1Y_{4-x}Gd_x$ ($x = 0, 1, 2, 3, 4$) composites were investigated. The thicknesses of $Al_{86}Ni_8Co_1La_1Y_{4-x}Gd_x$ ($x = 0, 1, 2, 3, 4$) ribbon alloy were 125 μm, 130 μm, 135 μm, 135 μm and 115 μm under 5 m/s rotate velocity, respectively. The corresponding XRD figures were shown in Fig. 3 and the results indicated that all of the phases were nearly amorphous structure. The choice of

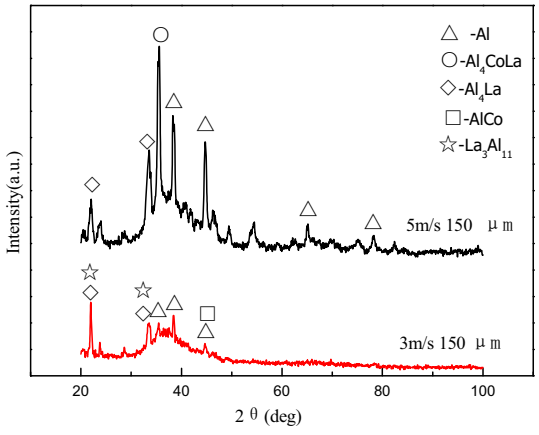

Fig. 1. XRD of $Al_{86}Ni_8Co_1La_5$ alloy ribbons prepared under 5 m/s and 3 m/s.

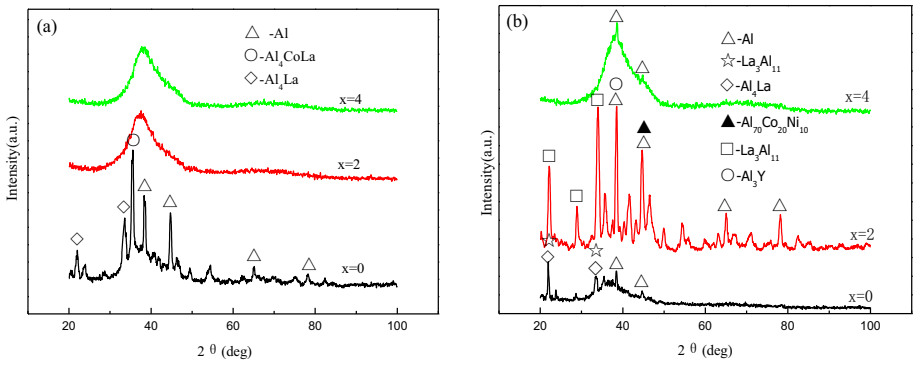

Fig. 2. XRD of $Al_{86}Ni_8Co_1La_{5-x}Y_x$ (x = 0, 2, 4) ribbons under 5 m/s (a) and 3 m/s (b).

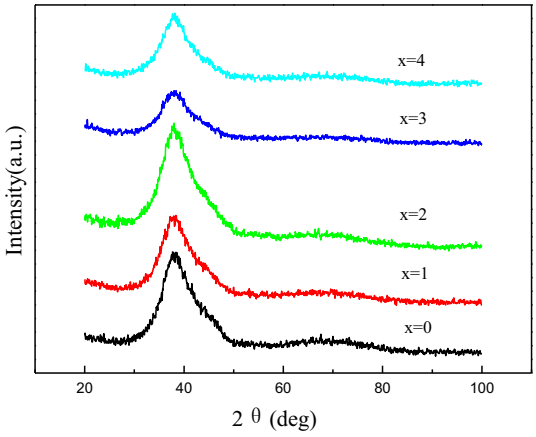

Fig. 3. XRD patterns of $Al_{86}Ni_8Co_1La_1Y_{4-x}Gd_x$ (x = 0, 1, 2, 3, 4) under roll speed 5 m/s.

$Al_{86}Ni_8Co_1La_1Y_{4-x}Gd_x$ materials is reasonable and satisfying. But it is difficult to distinct which component has the best amorphous form ability among 5 different composites.

In order to investigate further the effect of Gd on $Al_{86}Ni_8Co_1La_1Y_{4-x}Gd_x$, 3 m/s rotate velocity was considered and the XRD profiles of the quenched alloys were illustrated in Fig. 4. It showed that the x = 0 and x = 1 substitution produced the crystal peaks, which were judged as secondary phase α-Al using Jade 6.0 software. Surprising, no crystal peaks were observed for x = 2 substitution. But several crystal diffraction peaks were observed again

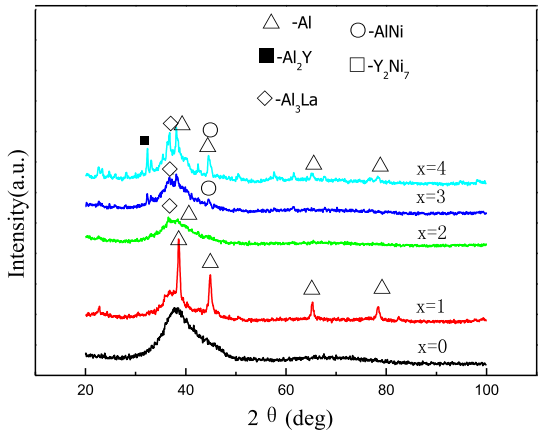

Fig. 4. XRD patterns of $Al_{86}Ni_8Co_1La_1Y_{4-x}Gd_x$ (x = 0, 1, 2, 3, 4, 5) under roll speed 3 m/s.

when the x = 3 and x = 4, and the peaks were also recognized as α-Al. This complicated reason will be explored in the future. In a word, XRD patterns (when x = 2) exhibited almost full amorphous states, and x = 0, 1, 3, 4 had weak α-Al peaks, demonstrating a mixed structure of crystal (very less) and amorphous phase (much more).

After the best chemical composite is confirmed, the TEM images of the $Al_{86}Ni_8Co_1La_1Y_2Gd_2$ were shown in Fig. 5 when roll velocity is 3 m/s. As seen in Fig. 5a and b, there was a typical amorphous scattering ring, which proved that $Al_{86}Ni_8Co_1La_1Y_2Gd_2$ was wholly amorphous structure. Therefore, $Al_{86}Ni_8Co_1La_1Y_2Gd_2$ had the best chemical composite in our investigations.

This phenomenon was induced due to the effect of both Y and Gd earth elements. Some reasons can be described briefly as follows. On the one hand, Al–Ni–Co–La–Y-Gd alloy is composed by 6 different elements (shown in Table 1). The radius differences of Ni–Y, Ni–Gd, Co–Y, Al–La, Al–Y and Al-G change from 20.6% to 31.1%, which are larger than 12% (Inoue's laws [19,20]). Therefore, Y and Gd can form the larger reticulation structure with other elements and further baffle some elements diffusion and moving. On the other hand, the least mix enthalpy of Ni–Y, Ni–Gd, Co–Y, Al–La, Al–Y and Al–Gd is about −22 kJ mol^{-1} and the largest

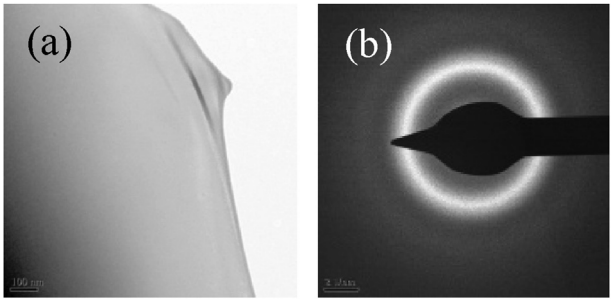

Fig. 5. Topography (a) and the corresponding micro area electron diffraction diagram (b) of $Al_{86}Ni_8Co_1La_1Y_2Gd_2$ alloy under 3 m/s.

Table 1
Atom size and mix enthalpy of composite elements for Al–Ni–Co–La–Y-Gd.

Elements	Al	Ni	Co	La	Y	Gd
Atom radius (nm)	0.143	0.124	0.125	0.183	0.180	0.180
melting point (Tm/°C)	660.4	1453	1495	920	1526	1312
Element - element	Ni–Y	Ni–Gd	Co–Y	Al–La	Al–Y	Al–Gd
Atom radius difference (%)	31.1	31.1	30.6	21.9	20.6	20.6
mix enthalpy (KJ·mol^{-1})	−31	−31	−22	−38	−38	−39

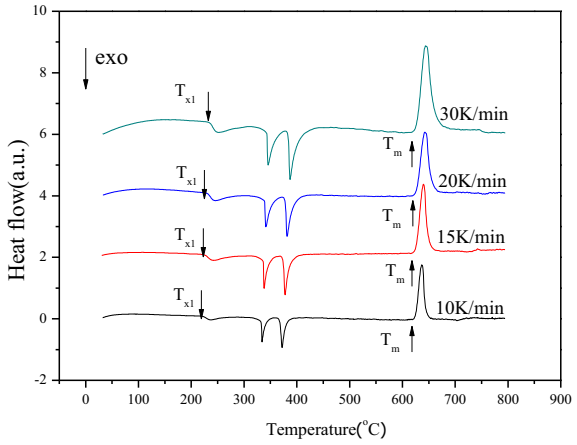

Fig. 6. DSC characteristics of the $Al_{86}Ni_8Co_1La_1Y_2Gd_2$ (roller speed of 5 m/s).

mix enthalpy is about −39 kJ mol^{-1}, wholly satisfy the condition of the larger mix enthalpy (Inoue's laws [19,20]).

3.3. DSC characteristic of Al-based amorphous alloys

Fig. 6 showed the DSC plot of the as-quenching $Al_{86}Ni_8Co_1La_1Y_2Gd_2$ alloy at various heating rates (10, 15, 20, 30 K/min) and the related DSC data were also summarized in Table 2. As seen in Fig. 6, the DSC curves exhibited clearly three exothermal peaks, corresponding to different crystallization stages during heating progress. It is well-known that the first peak corresponds to the crystallization of crystalline α-Al phase from amorphous phase and the temperature (Tx) is about 222 °C under 10 K/min. The second peak and the third peak is related to the crystallization growth phenomena under 10 K/min. As observed, the peak temperatures T_{p1} and T_{p2} are shifted to higher temperature with increasing heating rate, due to the presence of kinetic effects during the crystallization process.

Table 2
The data of DSC for $Al_{86}Ni_8Co_1La_1Y_2Gd_2$ samples (180 μm thickness, 3 m/s).

T_{x1} (°C)	T_{x2} (°C)	T_{x3} (°C)	T_{p1} (°C)	T_{p2} (°C)	T_{p3} (°C)	T_m (°C)	Heat rate (°C/min)
222	333	368	237	334	372	625	10
226	337	374	242	338	378	626	15
231	339	378	246	341	382	627	20
235	344	384	252	346	387	628	30

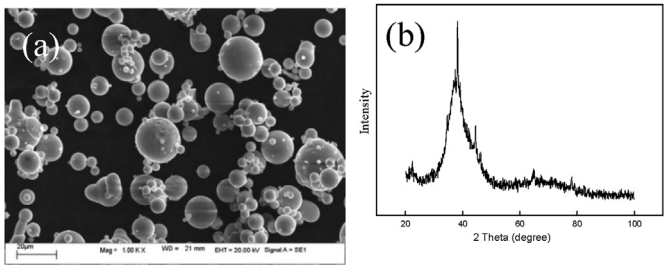

Fig. 8. Morphology (a) and XRD pattern (b) of Al-based amorphous powders.

It is important to know the activation energy of the crystallization process. The activation energy generally defined as the threshold value of energy above which the energy fluctuation is sufficient for the elementary reaction occurs, and it should have a characteristic constant value for each particular reaction. Using DSC results, the activation energy is calculated using Kissinger model, which are widely used for the calculation of activation energy in Finemet type alloys. The equation is listed as following:

$$\ln(T^2/\beta) = E/RT + C \quad (1)$$

where, β is the heating rate, T is the characteristic temperature, E is the crystallization activation energy, R is gas constant.

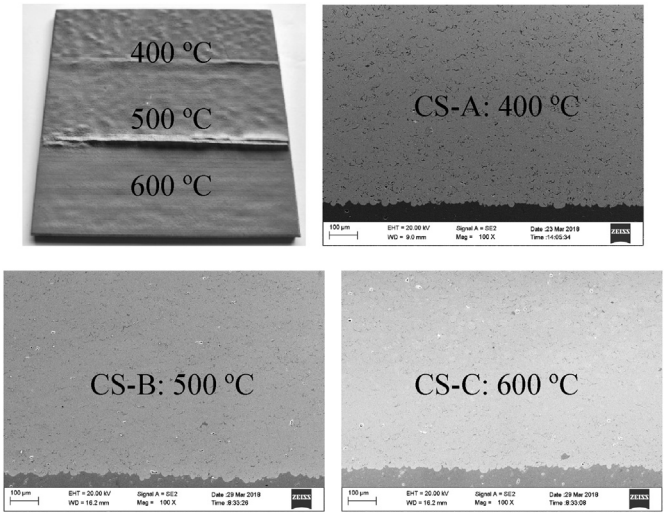

Fig. 9. Macro morphology and cross section of amorphous coatings.

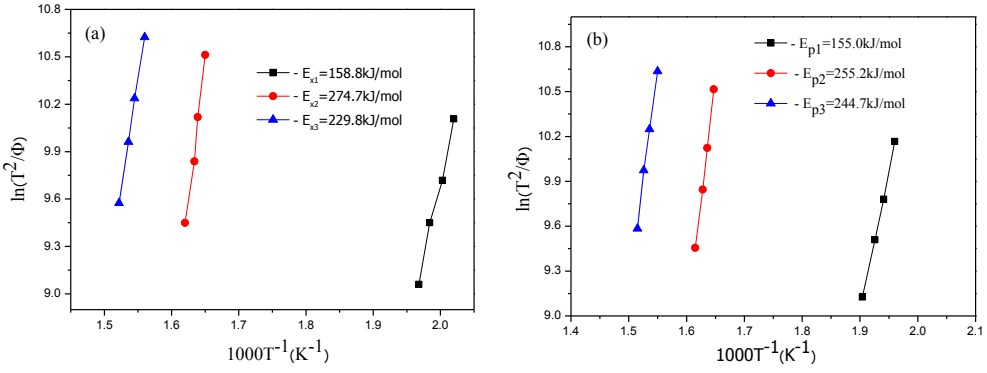

Fig. 7. Initial crystallization temperature T_{xi} (a) and the peak temperature T_{pi} (b) Kissinger curve of $Al_{86}Ni_8Co_1La_1Y_2Gd_2$.

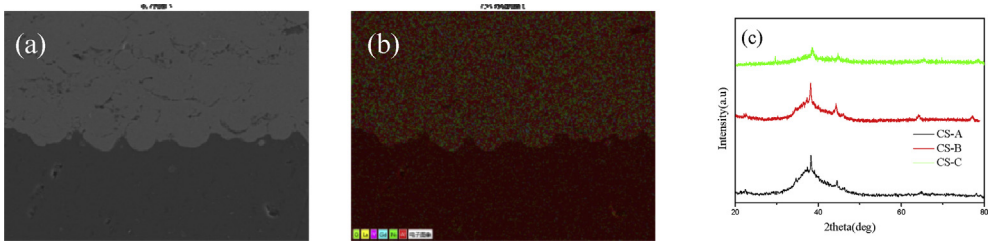

Fig. 10. The cross-sectional micro-structures (a) of the Al based amorphous coatings and the corresponding EDS maps (b) and XRD (c).

It can be seen that $\ln(T^2/\beta)$ has the better linear relation with T^{-1} (see Fig. 7). The nucleus activation energy E_{x1}, E_{x2} and E_{x3} ($Al_{86}Ni_8Co_1La_1Y_2Gd_2$, roller speed 3 m/s) is 158.8 kJ/mol, 274.7 kJ/mol and 229.8 kJ/mol, respectively. The growth activation energy E_{P1}, E_{P2} and E_{P3} is 155.0 kJ/mol, 255.2 kJ/mol and 244.7 kJ/mol, respectively. Here, the activation energies E_{a1} and E_{a2} indicate the participation of different phases in the first and second stage during continuous heating for the samples. Using Kissinger model-fitting method, Phan et al. find that their activation energy (E_{a1}) of Al based amorphous alloy is 313 kJ/mol. The α-Al phase crystallization activation energy (158.8 kJ/mol) of $Al_{86}Ni_8Co_1La_1Y_2Gd_2$ alloy is larger than that of $Al_{88}Ni_4Y_6Er_2$ (146.2 kJ/mol). The second peak (255.2 kJ/mol) is larger than that of $(Al_{80}Ca_8Li_6)_{97}La_3$ (the second peak is about 174.5 kJ/mol), demonstrating that $Al_{86}Ni_8Co_1La_1Y_2Gd_2$ amorphous alloy exhibits better thermal stability.

3.4. Characteristic of Al-based amorphous powder

$Al_{86}Ni_8Co_1La_1Y_2Gd_2$ amorphous powder was prepared using gas atomization and the technology detail were described in section 2.2. Powder's micro-graphs were shown in Fig. 8a. It can be observed that particles are between 3 μm and 23 μm, with an average size of about 18 μm. Moreover, the particles possess regular and smooth morphology, which is the typical character of gas atomization. Fig. 8b shows the corresponding XRD patterns of the Al-based gas atomization powder. The XRD patterns signify that there is a small quantity of crystal phase formation in these powders. The amorphous amount is evaluated and the value is about 86.2% using Pseudo-Voigt methods.

3.5. Al-based amorphous coatings prepared using CS technique

The $Al_{86}Ni_8Co_1La_1Y_2Gd_2$ amorphous powder was sprayed using the spraying temperatures of 400 °C, 500 °C, 600 °C, which were marked as CS-A, CS-B, CS-C, respectively. In Fig. 9, it easily shows that CS-C coatings have smooth surface and dense cross-sections at higher temperature. Usually, the area were collected, and then gray level difference analysis method was adopted and then entire image were measured, calculated and calibrated using Image J software. As a result, the porosities of CS-A, CS-B and CS-C were 4.8%, 1.3% and 0.5%, respectively. Therefore, CS-C has the lowest porosity in three kinds of parameters. Surprisingly, all of the thicknesses of them are also about 600 μm, which is speculated that $Al_{86}Ni_8Co_1La_1Y_2Gd_2$ amorphous powder has the suited hardness, plastic and toughness and suitable for cold spray.

Table 3
Element distribution for $Al_{86}Ni_8Co_1La_1Y_2Gd_2$ powder and coatings.

	Element	Al	Ni	Co	La	Y	Gd	O
Powder	at.%	86.0	8.0	1.0	1.0	2.0	2.0	0.0
As sprayed coatings	at.%	85.6	7.8	0.9	0.8	1.7	1.8	1.4

According to the EDS analysis (Fig. 10a, b and Table 3), the atomic proportion of the coatings is nearly equal to the nominal composition of the amorphous powder. There were very less oxygen atoms found in as-sprayed amorphous coatings, which are attributed to higher stabilization of powder and lower temperature spraying during cold spray. Besides, three kinds of coatings were analyzed according to XRD and the value of amorphous amount were about 84.7%, 82.8% and 80.2% using Pseudo-Voigt methods. The low oxygen content, very thick and dense structure will have good comprehensive properties, and the related properties will be investigated next.

4. Conclusions

Adding Y and Gd into $Al_{86}Ni_8Co_1La_5$ aluminum amorphous ribbons and the effects of two elements on phase structure, amorphous forming ability and thermal stability of $Al_{86}Ni_8Co_1La_5$ alloy were investigated. The results showed that the better additive amount for Y and Gd was both 2 at%. Therefore, $Al_{86}Ni_8Co_1La_1Y_2Gd_2$ was a better material which can form a whole amorphous strip although the roller speed was low to 3 m/s. $Al_{86}Ni_8Co_1La_1Y_2Gd_2$ amorphous powder was prepared easily in the gas atomization way and 86.2% amorphous proportion was kept. Meanwhile, amorphous powder was sprayed using cold spray and the as-sprayed coatings have thicker, dense structure and higher amorphous amounts. The thickness, porosity and amorphous amount of coatings was about 600 μm, 0.5% and 80.2% (CS–C), respectively. These results indicated that the design of $Al_{86}Ni_8Co_1La_1Y_2Gd_2$ amorphous powder is acceptable and $Al_{86}Ni_8Co_1La_1Y_2Gd_2$ amorphous powder could be used as a raw material for cold spray technology.

Conflicts of interest

The authors declare that there is no conflicts of interest.

Acknowledgement

The authors thank the Unite Fund (KZ041605114) and Civil Aircraft (MJ-2016-F-16) for the financial support for this research project.

References

[1] A. Inoue, N. Matsumoto, T. Masumoto, Mater. Trans. JIM 31 (1990) 493–500.
[2] N. Bassim, C.S. Kiminami, M.J. Kaufman, J. Non-Cryst. Solids 273 (2000) 271–276.
[3] D.V. Louzguine, A. Inoue, Mater. Lett. 54 (2002) 75–80.
[4] A. Inoue, S. Sobu, D.V. Louzguine, H. Kimura, K. Sasamori, J. Mater. Res. 19 (2004) 1539–1543.
[5] R.O. Suzuki, Mater. Sci. 18 (1983) 1195–1201.
[6] A. Inoue, M. Yamamoto, H.M. Kimura, et al., J. Mater. Sci. Lett. 6 (1987) 194–196.
[7] A.P. Tsai, A. Inoue, T. Masumoto, J. Mater. Sci. Lett. 7 (1988) 805–807.
[8] A. Inoue, K. Ohtera, T. Masumoto, Jpn. J. Appl. Phys. 27 (1988) L736–L739.
[9] A. Inoue, K. Ohtera, T. Zhang, et al., Jpn. J. Appl. Phys. 27 (1988) L1583–L1586.
[10] B.P. Suresh, R. Jha, M. Guzman, et al., Mater. Sci. Eng. A 658 (2016) 415–421.

[11] J. Henao, A. Concustell, I.G. Cano, et al., Mater. Des. 94 (2016) 253–261.
[12] S.B. Pitchuka, B. Boesl, C. Zhang, D. Lahiri, A. Nieto, G. Sundararajan, A. Agarwal, Surf. Coat. Technol. 238 (2014) 118–125.
[13] D. Lahiri, K. Puneet, G. Scudino, C. Zhang, V. Singh, J. Karthikeyan, N. Munroe, S. Seal, A. Agarwal, Surf. Coat. Technol. 232 (2013) 33–40.
[14] H.W. Zhang, J.Q. Wang, Z.Q. Hu, Mater. Rev. 15 (2001) 7–9 (in Chinese).
[15] T. Mika, M. Karolus, G. Haneczok, et al., J. Non-Cryst. Solids 354 (2008) 3099–3106.
[16] X.H. Fan, K. Yang, B. Li, W. Li, X. Wang, J. Xi'an Technol. Univ. 34 (2014) 146–151 (in Chinese).
[17] Y. Wang, Z.L. Zhan, X.H. Yu, L. Zhang, Z. Liu, L. Li, J.X. Liu, Trans. Mater. Heat Treat. 34 (2013) 12–16 (in Chinese).
[18] Z. Ling, L. Dechun, K. Shengzhong, Rare Met. Mater. Eng. 41 (2012) 1903–1906.
[19] M.A. Muñoz-Morris, S. Suriñach, M. Gich, M.D. Baro, D.G. Morris, Acta Mater. 51 (2003) 1067–1077.
[20] A.M. Vilardell, N. Cinca, I.G. Cano, A. Concustell, S. Dosta, J.M. Guilemany, S. Estradé, A. Ruiz-Caridad, F. Peiró, J. Eur. Ceram. Soc. 37 (2017) 1747–1755.